High Carbonate Alkalinity Lakes on Mars and their Potential Role in an Origin of Life Beyond Earth

Joel A. Hurowitz[1], David C. Catling[2], and Woodward W. Fischer[3]

Artist's reconstruction of Jezero Crater, Mars, as it may have looked billions of years ago when it was a lake. IMAGE CREDIT: NASA/JPL-CALTECH

1811-5209/23/0019-0037$2.50 DOI: 10.2138/gselements.19.1.37

The exploration of Mars has revealed that its ancient surface hosted lakes with a dazzling array of chemical and physical conditions and processes. The potential habitability of surface waters has driven studies aimed at understanding whether or not Mars once hosted life. High levels of atmospheric carbon dioxide are probable on early Mars, which means that lakes derived from weathering fluids could have contained substantial carbonate alkalinity. Recent studies show that lakes with high carbonate alkalinity are able to concentrate the phosphate and cyanide that are critical for molecular synthesis in the origin of life. While evidence for carbonate-rich Martian lakes remains limited, NASA's *Perseverance* rover may reveal clues about the past existence of such waters in Jezero Crater.

KEYWORDS: Mars; lake; alkaline; cyanosulfidic; origin of life

LAKES ON MARS

Mars was once awash in lakes (FIG. 1). A 2016 catalogue of all basins having geomorphic properties consistent with the former presence of a lake numbered over 400 (Goudge et al. 2016), and more recent efforts have added dozens more to the tally (Michalski et al. 2022 and references therein). Using crater counting techniques, and in one instance, in situ radiometric (K–Ar) age dating (Farley et al. 2014), constraints have been placed on the timing of the emplacement of these basins, and the sedimentary deposits contained in them. The upshot is that Martian lakes are ancient geological features, with most firmly planted in Mars' Noachian (from 4.1 to 3.7–3.5 Ga) or Hesperian (from the end of the Noachian to ~3.0 Ga) periods (Goudge et al. 2016). These are times when Mars' climate was likely characterized by a thicker atmosphere and warmer surface temperatures, at least episodically, compared with Mars today, as described in the next section.

Martian paleolakes exhibit an array of properties that mirror those of terrestrial lacustrine systems, including size variations, from basins larger than the Caspian Sea (Michalski et al. 2022) to diminutive playas (Grotzinger et al. 2005); open- and closed-system hydrology; and a range of catchment network development, from those clearly fed by abundant precipitation and/or snowmelt and runoff to those sourced by groundwater discharge (e.g., Fassett and Head 2008; Goudge et al. 2016). Most Martian lake basins were formed by bolide impacts, which created deep topographic holes for water and sediment accumulation. Thus, both physiography and climate evolution have restricted lake basins on Mars to its ancient crust, which is pockmarked by impact craters. While active debate continues regarding whether or not Mars' ancient climate and hydrology were able to support an ocean in the topographically low-lying region that defines the upper hemisphere of the Martian surface (FIG. 1), there is no question about the existence of paleolakes on Mars.

Martian paleolakes have been identified in topographic and imaging data collected from orbit, revealing drainage divides, river and stream networks, and features such as amphitheater-headed valleys that suggest erosion from groundwater discharge. Geomorphic features of running water are frequently connected to basins that received meteoric and/or groundwater. In many, but not all cases, these basins were filled by sedimentary deposits (e.g., alluvial fans, deltas, lake sediments), further suggesting the former presence of standing water. Perhaps one of the most spectacular examples of a Martian lake system is marked by the fluvio-deltaic deposit contained within Jezero Crater (FIG. 2), the landing site of NASA's 2020 Mars rover, *Perseverance*. Spectroscopic analyses collected from orbit at high spatial and spectral resolution reveal the mineral phases transported to, and formed in, these ancient lake systems (e.g., Horgan et al. 2020), including detrital igneous minerals, phyllosilicates, and a rich variety of salt minerals. Ground-based observations from inside the Gusev, Gale, and Jezero paleolakes collected by the Mars Exploration Rover (MER) *Spirit*, the Mars Science Laboratory (MSL) *Curiosity*, and the *Perseverance* rover, respectively, have added detailed sedimentological, chemical, and mineralogical data that enable reconstruction of the depositional and diagenetic history of sediment accumulation, and the astrobiological potential of lakes on early Mars (McLennan et al. 2019).

Evidence for ancient lakes on Mars represents an interesting point of divergence with the terrestrial geological record. Earth's history is primarily written in the sedimentary record of long-lived marine basins, whereas lakes are geologically ephemeral and rarely preserved in deep time. Because plate tectonic processes are not operative on Mars, ancient paleolake basins are frequently and spectacularly

1 Department of Geosciences
Stony Brook University
Stony Brook, NY 11794, USA
E-mail: joel.hurowitz@stonybrook.edu

2 Department of Earth and Space Sciences
University of Washington
Seattle, WA 98185, USA
E-mail: dcatling@uw.edu

3 Division of Geological & Planetary Sciences
California Institute of Technology
Pasadena, CA 91125, USA
E-mail: wfischer@caltech.edu

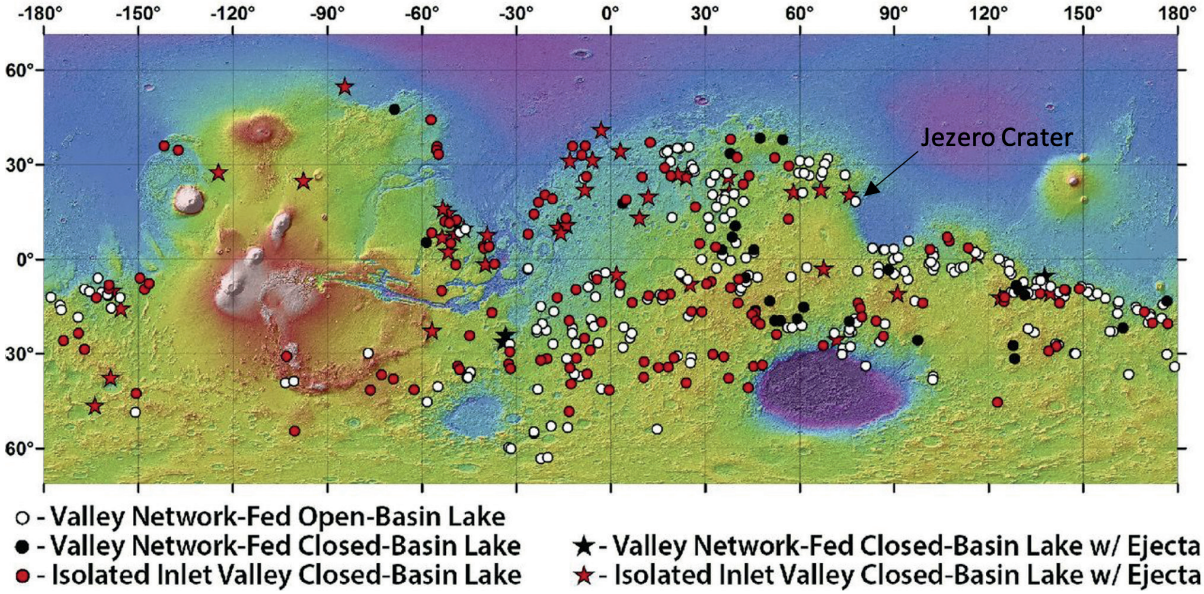

Figure 1 Distribution of paleolakes on Mars from Goudge et al. (2016). Open- and closed-basin valley network-fed lakes (black and white symbols, respectively) were primarily formed earlier in Martian geological history, prior to 3.7 Ga. Closed-basin paleolakes with isolated inlet valleys (red symbols) primarily formed subsequent to the era of major valley network formation, after 3.7 Ga. Closed-basin lakes indicated by stars are hosted by craters with continuous ejecta deposits or have inlet valleys that incise continuous ejecta deposits of nearby craters, indicating more recent activity than their counterparts that are mapped with circular symbols. The location of Jezero Crater (white circle with label) is indicated. The background shows the Mars Orbiter Laser Altimeter (MOLA) gridded topography, in which white represents the highest elevations and purple the lowest, overlain on a MOLA-derived hillshade map.

well preserved (Fig. 2). With quiescent tectonics, craters established a local base level for accumulation, were infilled by water and sediment, and were subsequently spared the uplift, erosion, and removal that destroy paleolake records on Earth. In Mars' cold, dry climate, which has dominated for perhaps the past 3 billion years, ancient paleolake deposits are slowly winnowed away by the wind at rates of microns per year (Farley et al. 2014). However, such rates, integrated over billions of years, can cause kilometers of local/regional erosion or deposition.

BOUNDARY CONDITIONS

Mars' hydrosphere ultimately derives its properties from interactions with the atmosphere and the rocky crust of the planet. Therefore, it is useful to review what is known about these important reservoirs to assess how the boundary conditions they set might have led to alkaline conditions in ancient Martian lakes and, in particular, whether those conditions were conducive to prebiotic synthesis.

Climate and Atmospheric Composition

The details of Mars' climate evolution remain an area of active and ongoing research (e.g., reviewed by Catling and Kasting 2017) with major questions centering on the following. (1) What were the drivers and rates of atmospheric loss that caused Mars to evolve from a warmer and wetter planet, with a thicker atmosphere, to a cold, arid planet with a thin atmosphere with a global average surface pressure of ~6 mbar? (2) What conditions were required to provide sufficient climate warming to enable liquid water to flow and pond at the surface of Mars billions of years ago, when its atmosphere was thicker? For years, this issue has confounded researchers, who have recognized that the same faint young Sun (FYS) problem that must have affected surface temperatures on the early Earth were even harder to overcome on Mars at a distance of 1.5 AU from the Sun.

We highlight two proposed warming scenarios from the recent literature to illustrate how advances in Mars exploration have led to sophisticated mechanisms to solve the FYS problem. First, motivated by discoveries of significant variations in the redox state of secondary minerals in Martian clastic sedimentary rocks in Gale Crater, Wordsworth et al. (2021) proposed that Mars experienced significant stochastic variations in surface temperature driven by the episodic production and accumulation of H_2, which is a significant greenhouse gas at high concentrations in a CO_2 atmosphere, via metal-rich bolide impacts, crustal alteration processes, and volcanism. Geologically brief (10^4–10^5 years), warm, reducing (i.e., high pH_2) intervals would have alternated with colder, more oxidizing intervals as H_2 was subsequently lost to space via escape from the upper atmosphere. As the mechanisms driving H_2 production and climate warming became less frequent, and the total atmospheric pressure declined, this model predicts that warm intervals should have become less frequent over time. Second, Kite et al. (2021) proposed that high-altitude water ice clouds on a generally arid planet with patchy surface ice deposits can give rise to warm surface temperatures over relatively long intervals (>10^6 years) without calling on the introduction of reduced greenhouse gases, like H_2, into a thick (≥1 bar) atmosphere. Further research will likely identify additional mechanisms capable of warming early Mars, and these recent efforts highlight the need to find warming solutions that simultaneously satisfy the FYS paradox and fit the growing amount of geological and geochemical data that speak to the chemistry of aqueous environments on the ancient surface of Mars and the history of atmospheric escape from the planet.

Given the ongoing nature of the debate over Mars climate evolution and the long-term changes in the composition of its atmosphere and hydrosphere, it is useful to simplify the problem as it relates to Martian lakes by recognizing that Mars' atmosphere is ~95% CO_2 today and likely has been CO_2-dominated throughout its geological history (leaving

open the possibility of a significant early N_2 partial pressure, e.g., Hu and Thomas 2022). Thus, whenever a given lake was present on Mars, and assuming that its surface was ice-free, its water chemistry would have been significantly influenced by dissolved inorganic carbon (DIC) derived from the atmosphere.

The Nature of the Martian Crust

Mars is separated into two major physiographic provinces: a heavily cratered, high-standing southern hemisphere, where paleolakes are inferred, and a low-standing northern hemisphere that exhibits a smoother average surface topography, possibly reflecting coverage by a volcanic or sedimentary veneer that drapes and infills what was once rough, cratered topography (Fig. 1). Mars' surface is also characterized by large volcanic constructs, such as the Tharsis Montes, which reflect the long-term accumulation of lavas and magma over mantle hot spots. Measurements of the chemical composition of Mars' exposed crust from orbital gamma-ray spectroscopy, in situ chemical measurements of Martian rock and regolith, and laboratory measurements of Martian meteorites indicate that its average composition is equivalent to that of subalkaline Fe-rich basalt, with the primary mineralogy dominated by plagioclase feldspar, high- and low-Ca pyroxenes, olivine, Fe–Ti oxides, and volcanic glass (McLennan et al. 2019). This crustal composition represents yet another point of divergence from the Earth, which has a bimodal character: buoyant continental crust of mostly granodioritic composition and denser oceanic crust of mostly basaltic composition. Orbital and in situ measurements reveal considerable regional diversity in the chemical and mineralogical properties of Martian igneous rocks, from evolved, K_2O-rich alkaline igneous compositions to ultramafic olivine cumulates, such as those recently discovered in the floor of Jezero Crater (Liu et al. 2022). These variations are thought to reflect fractional crystallization processes within regional magmatic systems, and do not require operation of the same plate tectonic processes that gave rise to the complex rock cycle and bimodal crust of the Earth.

The generally mafic composition of the Martian crust influences the sediments, secondary minerals, and water chemistry that result from the interaction of meteoric water and rock on Mars. Excellent examples of the unique properties of Martian clastic and chemical sedimentary rocks, and the fluids they formed in, can be found at Meridiani Planum and Gale Crater, the landing sites of the MER *Opportunity* and MSL *Curiosity* rovers, respectively. At Meridiani Planum, hundreds of meters of sandstones (and rare mudstones) of the "Burns formation" are widely, though not universally, interpreted to have formed in an evaporitic desert dune–playa environment (Grotzinger et al. 2005). The sand grains in the Meridiani Planum sandstones are composed of roughly equal parts weathered basaltic siliciclastic detritus and Fe^{3+}–Mg–Ca sulfate minerals and amorphous silica, which also form the cementing agent that binds the sand grains together. This chemical-siliciclastic deposit shows evidence for multiple episodes of diagenetic overprint, which resulted in the production of millimeter-scale spherical hematite concretions found throughout the deposit (McLennan et al. 2019). The ubiquitous presence of the ferric sulfate mineral jarosite (~10 wt.%) throughout the Burns formation provides strong evidence for sulfate-rich, low-pH water conditions, the origin of which is a matter of ongoing debate (e.g., Kite and Daswani 2019). The terrestrial rock record has no complete analogue to all of the unique mineralogical, chemical, and sedimentological attributes of the Burns formation on Mars, though partial analogues provide useful guidance (e.g., Baldridge et al. 2009).

Gale Crater is also filled with kilometers-deep siliciclastic sedimentary rock, predominantly made of lacustrine mudstones, along with sandstones and conglomerates formed in deltaic, riverine, and aeolian settings. While

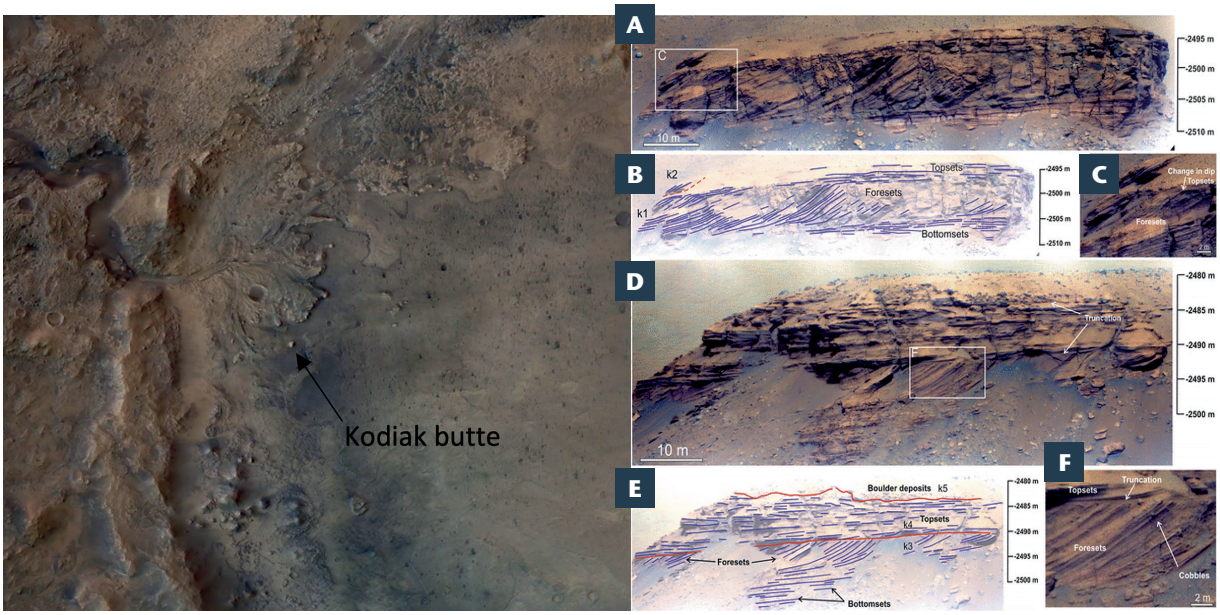

Figure 2 (**left**) Color image of the delta in Jezero Crater taken by the High-Resolution Stereo Camera aboard the European Space Agency Mars *Express* orbiter (ESA/DLR/FU-Berlin). (**A–F**) Stratigraphic relationships observed in Kodiak butte, which is an isolated erosional remnant of the delta imaged by the *Perseverance* rover shortly after landing in Jezero Crater. Reproduced from Mangold et al. (2021) with permission from The American Association for the Advancement of Science. Elevation scales are inferred from a digital elevation model and have systematic uncertainties of ±2 m. White boxes indicate regions shown in more detail in other panels. (**B**), (**E**) Interpreted line drawings of the main visible beds (blue lines for individual beds and red lines for discontinuities), overlain on the images from (**A**) and (**D**). (**C**) Zoomed image of k1 showing the change in dip from sub-horizontal beds (topsets) to inclined beds (foresets). (**F**) Zoomed image of the foresets in k3. This unit has a coarse texture with several cobble-size clasts. The erosional truncation of k3 by k4 is labeled.

the Gale section, still being actively explored with the MSL *Curiosity* rover, provides evidence for multiple stages of deposition, erosion, and diagenesis, the predominant theme that has emerged over the past decade of investigation is that Gale Crater was infilled by lacustrine mudstones over a long (~10^4–10^6-year) integrated period of deposition after the crater was formed at ~3.5 Ga (Grotzinger et al. 2015). The mineralogy of these mudstones is dominated by detrital mafic minerals, phyllosilicates, secondary oxides, Ca–Mg sulfates, and a surprisingly large and omnipresent complement of X-ray amorphous materials, which may represent a combination of detrital volcanic glass and poorly crystalline authigenic and alteration products (Rampe et al. 2020). Taken together, the mineralogy of these deposits supports the inference that lake waters in Gale Crater were circum-neutral in pH, with substantial evidence for redox disequilibrium, and indicates that the lacustrine deposits were considerably impacted by multiple episodes of diagenesis under variable conditions during burial and lithification. Cold, wet, basalt-hosted fluvio-lacustrine settings, such as those found in Iceland, appear to provide a useful terrestrial process analogue to the conditions of sediment generation in Gale Crater (Thorpe et al. 2021).

ACHIEVING HIGH CARBONATE (OR TOTAL) ALKALINITY IN A MARTIAN LAKE

Given the boundary conditions described above, it is possible to provide a general assessment of the likelihood that Martian lakes could have achieved high alkalinity conditions. Here, it is useful to describe alkalinity in the two senses of the term in common usage (see this issue's *Toolkit*): alkaline as it is used in the colloquial sense to describe water pH values significantly higher than pH = 7, and alkaline as it refers to the significant concentrations of acid-neutralizing ions (i.e., the conjugate bases of weak acids, typically HCO_3^-, CO_3^{2-}, and OH^-, expressed in equivalents of charge per kilogram of water) that alkaline systems tend to accumulate. In terrestrial alkaline lake systems, the two definitions of alkalinity often go hand-in-hand because the lake water has both high pH and high concentrations of acid-neutralizing ions, especially those derived from DIC. Thus, total alkalinity is dominated by the carbonate alkalinity of HCO_3^- and CO_3^{2-} ions. As we will see for Martian lakes, these two conceptual descriptions of alkalinity do not necessarily have to be linked because a lake could have high carbonate alkalinity and yet have pH < 7 if pCO_2 was high on early Mars.

Numerous efforts have been made to estimate likely chemical compositions for ancient Martian waters based on observational evidence, terrestrial analogues, and experimental and modeling studies. All such studies make assumptions and trades to circumvent the limitations imposed by orbital and in situ measurement capabilities that prevent reconstruction of a complete chemical system, differences between the kinetics of laboratory and field processes, or non-unique model outcomes. This is especially true in the case of Mars, where we are trying to reconstruct multi-billion-year-old paleoenvironmental conditions on a planet that is roughly 150 million kilometers from Earth! Nevertheless, these types of studies have identified general mechanics and provided valuable insights into the chemical conditions and potential habitability of Martian waters in a variety of surface and subsurface settings.

Less attention has been paid to the specific topic of alkalinity, likely owing to a paucity of useful analogues or experiments with the specific properties required for Mars, i.e., basaltic protolith (with its own unique average chemical and mineralogical properties), high pCO_2, and P–T conditions close to standard temperatures (25 °C) and pressures (1 atm). Fortunately, the body of literature that is concerned with the sequestration of atmospheric CO_2 in basaltic rock as a geoengineering solution to mitigate against climate change provides a basis from which we can draw insights. Here, a particularly useful pair of studies that can be adapted to understand water alkalinity on Mars are highlighted. Gysi and Stefánsson (2011) built a reaction path model that was constructed using the software package PHREEQC to simulate the kinetically controlled dissolution of basaltic glass derived from the Stapafell Volcano in western Iceland in the presence of Icelandic spring water. A new thermodynamic dataset for secondary minerals relevant to water–rock reactions under the conditions being modeled was also presented. This dataset is based on observed secondary phases formed in the natural environment in Iceland, and includes a suite of Fe–Mg–Ca carbonates (including solid solutions), phyllosilicates, silica polymorphs, zeolites, hydrated Al-silicates, and Al- and Fe-oxyhydroxides. Crucially, their simulations were validated against experimental data, presented in Gysi and Stefánsson (2011, 2012), in which the Stapafell volcanic glass was reacted with Icelandic spring water under high-pCO_2 conditions (1–13 bar CO_2), a low initial water-to-rock ratio (1–10), and relatively low temperatures (40 °C), not much above ambient temperature. Thus, their experimentally validated model presents a useful comparison point for understanding basalt–water reactions and water alkalinity on Mars under high pCO_2 and near-ambient temperature conditions.

To illustrate the weathering processes operating when meteoric water interacts with Martian basaltic crust in a lake catchment, we completed a suite of geochemical model calculations. The reaction path model described above was adapted to run in the React component of the Geochemist's Workbench (GWB v.15) and used in a simulation in which 200 g of Stapafell glass, having an initial geometric surface area of 50 cm^2/g, reacts with 1 L of Vellankatla spring water at 40 °C at a pCO_2 of 1.2 bar under both closed- and open-system conditions. No O_2 is present in the model system, and the only ferric iron present is that sourced from the Stapafell glass. The closed-system simulation is identical to that used to produce Figs. 10 and 12 in Gysi and Stefánsson (2011). Here, however, the focus is specifically on the evolution of alkalinity and pH and the concentrations of Fe^{2+}, Mg^{2+}, and Ca^{2+} as the water–rock reaction proceeds. The only significant change made to the model presented here was to also consider the production and dissolution of brucite ($Mg(OH)_2$), portlandite ($Ca(OH)_2$), and $Fe(OH)_2$, using solubility data from the GWB thermo.dat database, to provide constraints on Fe^{2+}, Mg^{2+}, and Ca^{2+} concentrations at high pH.

The model results are illustrated in Fig. 3A and 3B. In Fig. 3A, the variation in the total alkalinity (TA), carbonate alkalinity (CA = $[HCO_3^- + 2CO_3^{2-}] - H^+$), and individual species that contribute to the total alkalinity are displayed as a function of pH. Here, we define TA = $([HCO_3^- + 2CO_3^{2-} + OH^-] - H^+)$, which is an approximation that neglects species such as $B(OH)_4^-$, for which we have no data. Also shown are the experimental results from Gysi and Stefánsson (2011, 2012), which were conducted under conditions similar to those of the closed-system model, to assess the degree of correspondence between model and experiment. The initial state of the system is characterized by low pH and low total alkalinity, resulting from high pCO_2, which in turn imparts a high concentration of DIC (as $CO_2(aq)$ and H_2CO_3), but does not contribute to the alkalinity. The pH and alkalinity of the system then increase as H^+ is consumed through water–basalt reactions, releasing cations to maintain the

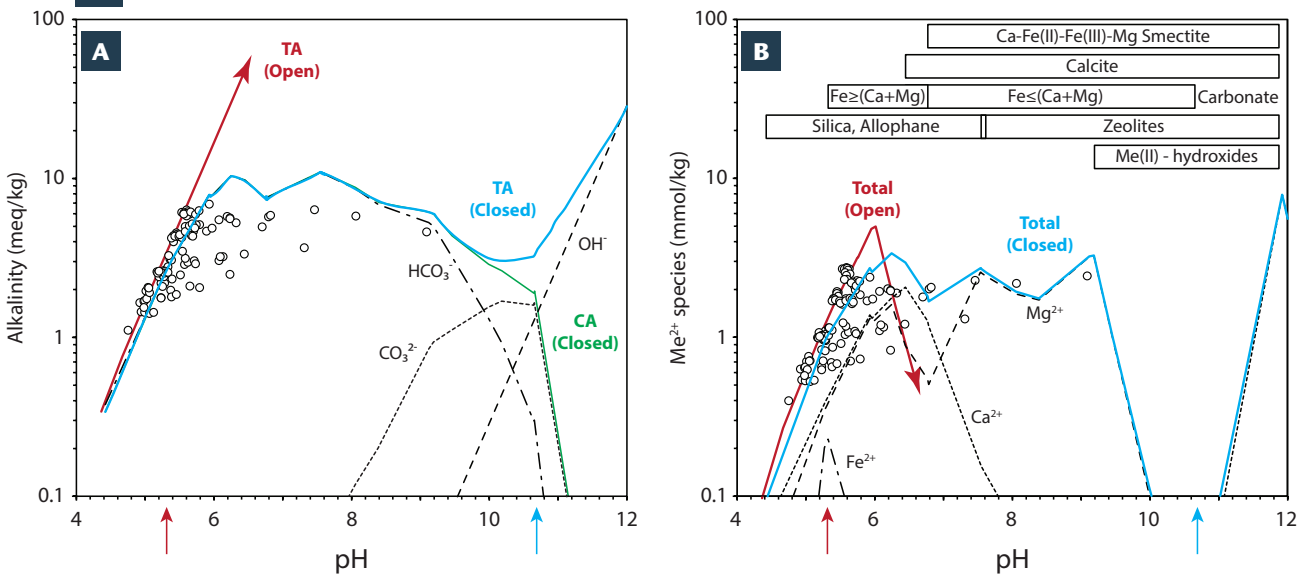

Figure 3 Evolution of (**A**) fluid pH, total alkalinity (TA), and carbonate alkalinity (CA) and (**B**) dissolved Me^{2+} cations during the reaction between basaltic glass and CO_2-charged (1.2 bar) water at 40 °C. White circles represent measurements of the same parameters in experimental fluids from Gysi and Stefánsson (2012). The blue lines in both panels represent the modeled total alkalinity ($[HCO_3^-] + 2CO_3^{2-} + OH^-] - H^+$) and total Me^{2+} concentration ($Fe^{2+} + Mg^{2+} + Ca^{2+}$) under closed-system conditions in which CO_2 is not replenished during water–rock reactions. In (**A**), the green line represents the contribution to total alkalinity from dissolved inorganic carbon species (= $[HCO_3^- + 2CO_3^{2-}] - H^+$). The dashed, dash–dot, and dotted lines show the individual concentrations of species that contribute to alkalinity and total Me^{2+} for the closed-system model. In both panels, the red lines represent the outcome of modeling the same system under the assumption that it is open with respect to CO_2 recharge. At the top of (**B**), the bars denote where in the closed-system simulation particular groups of secondary minerals have precipitated and remain stable. Arrows along the pH axes show the open (red) and closed (blue) system fluids used to calculate the fluid mixture compositions shown in Table 1.

charge balance, and the DIC speciation adjusts to form HCO_3^-. As the pH continues to increase from ~6 to ~10, the total alkalinity level stabilizes at ~10 mEq/kg, balancing the charge from dissolved cations, whose concentrations are set by secondary mineral precipitation. Above pH ~10, the carbonate alkalinity (CA) drops off dramatically as the system's DIC is fully consumed by carbonate mineral precipitation. From this point forward, pH and TA continue to increase as the water–rock reaction proceeds and OH^- becomes the dominant contributor to TA. Thus, over the course of this closed-system simulation, which might be thought of as representing the evolution of groundwater as it moves from its recharge point into the subsurface along aquifer flow paths, the fluid evolves from a low-pH, low-TA (and -CA) state, to an intermediate-pH, high-TA (and -CA) state, to a high-pH, high-TA (low-CA) state.

The open-system simulation, in which CO_2 is replenished as it dissolves into the fluid and is drawn out by carbonate mineral precipitation, initially behaves like the closed-system, with low pH and low TA (and CA), but then diverges and evolves along a different trajectory; one in which CA continues to increase unchecked as the water–basalt reaction consumes H^+, HCO_3^- is formed, and DIC is replenished. This open-system simulation can be thought of as representing the evolution of surface waters as they move from their recharge point to a terminal sink while in constant communication with a CO_2-rich atmosphere. The open-system simulation highlights an important example of what may be a uniquely Martian surface water type—one that has a pH below 7 but is accompanied by high carbonate alkalinity. On Earth, such fluids are only found in association with water influenced directly by magmatic CO_2 degassing, such as Lake Nyos, hosted in a caldera in Cameroon, which has pH < 6 below an upper chemocline level, and yet has lake floor sediments of siderite ($FeCO_3$), amorphous silica, and kaolinite clay (e.g., Kusakabe et al. 2019).

Figure 3B presents the results of these same simulations, but in this case, the variations in the divalent metal cation concentrations ($Me^{2+} = Fe^{2+} + Mg^{2+} + Ca^{2+}$) are displayed as a function of pH. It is the relative abundance of these divalent cations to CA that determines whether or not an alkaline lake will form in a hydrologically closed basin; this is because the precipitation of Ca-, Mg-, or Fe-carbonate salts will remove two moles of total alkalinity per mole of Me^{2+} by either

$$Me^{2+} + \mathbf{HCO_3^-} = MeCO_3 + \mathbf{H^+}$$

or

$$Me^{2+} + \mathbf{CO_3^{2-}} = MeCO_3,$$

where **bold** indicates species consumed or produced to lower the total alkalinity.

Thus, if $Me^{2+} > [2TA]$, alkalinity will be consumed during evaporation and the fluid will evolve toward a low-pH, low-TA condition, whereas if $Me^{2+} < [2TA]$, Me^{2+} will be consumed during evaporation and the fluid will evolve toward a high-pH, high-TA condition (Tosca and Tutolo 2023 this issue). Accordingly, it is important to evaluate the behavior of Me^{2+} cations during water–rock reactions so that their abundance relative to the alkalinity can be evaluated.

As shown in Fig. 3B, Fe^{2+}, Mg^{2+}, and Ca^{2+} have a number of sinks in the closed-system reaction path model, including smectitic clays, calcite, mixed cation carbonate minerals, zeolites, and, at the highest pH levels, hydroxides of Mg, Ca, and Fe^{2+}. In fact, cation concentrations are only able to build up to millimolar levels during the early stages of the simulation, when the initial low pH of the system is being modified by the exchange of H^+ for Me^{2+} and secondary precipitates are dominated by silica, allophane, and Fe^{3+}-hydroxide. After this point, from pH ~6 to 10, total Me^{2+} levels plateau as they are consumed through precipitation. Above pH ~10, brucite ($MgOH_2$) precipitation removes

the remaining Mg^{2+} from solution and Ca^{2+} briefly increases between pH 11 and 12 as the basaltic glass continues to dissolve until $Ca(OH)_2$ achieves saturation. As before, the open-system simulation evolves along a different trajectory; one in which Me^{2+} species increase in concentration until a pH of ~6, above which carbonate mineral precipitation causes the total Me^{2+} concentration to drop precipitously. After this point, increasing alkalinity in the model is mostly charge-balanced by monovalent Na^+ and lesser K^+ (not shown in Fig. 3).

These simulations of open- and closed-system fluid chemistry set up interesting possibilities for the interaction between ground and surface waters on Mars. If we imagine surface waters as being represented by the open-system simulation pathways in Fig. 3A and 3B, and groundwaters as being represented by the closed-system simulation pathways, then we have a means to produce distinct fluid chemistries as meteoric water interacts with basalt in settings that are either well or poorly connected to the atmosphere. In an endmember sense, surface fluids could be characterized by lower pH (<6–7) and variable CA (dominated by HCO_3^-) and Me^{2+} concentrations, depending on the kinetics of water–rock reactions and associated secondary mineral precipitation. In contrast, subsurface fluids could be characterized by high pH (as high as 11–12), high TA (dominated by OH^-), and low Me^{2+} concentrations. The location where one might expect such fluids to meet is at the sediment–water interface beneath a lake. This mixing zone forms the locus for many interesting mineralization reactions, such as those described in Tosca et al. (2018) for the specific case of authigenic magnetite precipitation in Gale Crater, and possibly for carbonate mineralization on Mars. Indeed, the composition of mixtures (produced using React) derived from the two fluids having the lowest and highest TA/Me^{2+} ratios (Table 1, with the endmembers also shown by the arrows in Fig. 3A and 3B) indicates that all of the mixed compositions are saturated with respect to carbonate minerals. This scenario is analogous in many respects to processes that drive carbonate mineralization in terrestrial alkaline lake systems (e.g., Ingalls et al. 2020), and provides a testable hypothesis to explain the observation that carbonate-rich strata are concentrated in marginal deposits that exist between the crater rim and the delta (Fig. 2) in Mars' Jezero Crater (Horgan et al. 2020).

It is worth noting that temperature conditions must also have played an important role in dictating the style of mineralization resulting from water–rock reactions on Mars. The temperature conditions (40 °C) illustrated in Fig. 3A and 3B indicate that carbonate minerals are a significant part of the secondary mineral assemblage, but the same model run at lower temperatures might result in a different outcome. For example, Li-isotopic measurements of cave speleothems across Pleistocene glacial intervals (Pogge von Strandmann et al. 2017) indicate that clay mineral precipitation from water–rock reactions is strongly favored during glacial periods, a result of the decreased solubility of clays at cold temperatures. Under such conditions, carbonate precipitation might be disfavored as a result of the inverse relation between carbonate mineral solubility and temperature, and the loss of Me^{2+} to clays. Accordingly, in the few locations where carbonates are present on Mars, their presence may not just be a signal of waters with high CA but also of warmer temperatures. This is an area of inquiry that would be well served with additional research to sort out the effects of temperature on parameters such as the primary mineral dissolution rate, secondary mineral solubility, and gas solubility under Mars-relevant conditions.

Perhaps one of the most surprising aspects of the model results presented in Fig. 3A and 3B is that, over the course of both the closed- and open-system simulations, the concentration of alkalinity is higher than that of the divalent metal cation species. In fact, calculations of TA/Me^{2+} reveal that this ratio remains above 2 for the entirety of both simulations, except for a narrow window early in the open-system simulation where the Fe^{2+} concentration is at its maximum (Table 1). This suggests that almost any fluid derived from these water–rock reaction pathways would evolve toward high pH and high alkalinity if subjected to evaporative concentration (Tosca and Tutolo 2023 this issue). Given the apparent paucity of widespread carbonates (Ehlmann and Edwards 2014) and/or minerals that might be expected to form in association with the evaporation of high-pH, high-TA waters on Mars (e.g., Na-carbonates, calcite, hydrous Mg-carbonates), it would appear that our analysis of Martian fluid chemistry is missing a critical ingredient. One possibility is that dissolved sulfate appears to have played an outsized role in determining the fluid chemical properties of waters in Martian surface and subsurface environments (McLennan et al. 2019). The oxidation of reduced sulfur species, in the form of SO_2 from volcanic gas sources and/or S^{2-} from sulfide minerals, provides the primary source of this sulfate. If present at concentrations significantly higher than indicated by the Icelandic spring water in our model (1.5×10^{-2} mmol/L, Table 1), the addition of H^+ derived from S-oxidation can have the effect of decreasing TA by lowering pH, increasing the concentration of HSO_4^- (itself an H^+ donor), and removing CA through the protonation of bicarbonate. Hydrolysis caused by iron oxidation and ferric iron mineral precipitation is also thought to have played an important role in lowering TA through acid production (McLennan et al. 2019 and references therein). It is therefore possible that a combination of S-sourced acids and Fe-oxidation tipped the TA/Me^{2+} ratio in many Martian watersheds to values ≤ 2, making alkaline lake systems on Mars the exception, rather than the rule.

PREBIOTIC CHEMISTRY IN MARTIAN LAKES – CHALLENGES AND PROSPECTS

Martian lakes are, by their very nature, exciting prospects for exploration in the context of the search for life on other worlds. Lakes represent habitable environments, with abundant liquid water and access to light and chemical energy sources that could have sustained primitive biology on the ancient surface of Mars (Grotzinger et al. 2015; Michalski et al. 2022). It is no surprise then that three (*Spirit*, *Curiosity*, and *Perseverance*) of the five NASA rovers sent to Mars landed in craters thought to have hosted lakes, and that data from a fourth rover (*Opportunity*) ultimately showed that rock deposits associated with ancient playa lakes were present at its landing site. All have resulted in the discovery of habitable environments of one kind or another, which motivates the search for signs of life at these landing sites, and the eventual return of samples from Mars for study in terrestrial laboratories. But might Martian lakes also reveal something about the origin of life in the Solar System?

The chemistry associated with life's origins on Earth has received much attention over the years, and an exhaustive review is not possible here. Suffice to say that there is a great diversity of opinion about whether life started as a result of atmospheric chemistry in a reducing atmosphere (i.e., CH_4- and HCN-rich, like in the Miller–Urey experiment), as a result of organic synthesis reactions occurring in association with hydrothermal systems at the seafloor or near the Earth's surface, or in surface environments associated

Table 1 MODELED PROPERTIES OF MARTIAN RIVER WATER, GROUNDWATER, AND THEIR MIXTURES.

Analyte*:	pH	H_4SiO_4	Al^{3+}	Fe^{2+}	Fe^{3+}	Mg^{2+}	Ca^{2+}	Na^+	K^+	DIC	SO_4^{2-}	Cl	HCO_3^-	CO_3^{2-}	TA	TA/Me^{2+}	$Fe(CN)_6^{4-} \geq Fe^{2+}$
Groundwater**	10.7	0.12	0.11	5.2×10^{-5}	1.6×10^{-2}	5.9×10^{-3}	1.1×10^{-2}	6.15	0.20	2.74	1.5×10^{-2}	0.12	0.39	1.69	5.48	328	---
5% RW‡	10.2	0.10	6.5×10^{-2}	2.4×10^{-4}	4.4×10^{-3}	6.4×10^{-4}	3.5×10^{-3}	5.90	0.19	3.80	1.5×10^{-2}	0.12	1.43	1.70	9.58	2,170	Yes†
10% RW	9.17	0.13	8.1×10^{-3}	2.0×10^{-4}	5.8×10^{-4}	9.9×10^{-4}	8.4×10^{-3}	5.54	0.18	5.32	1.5×10^{-2}	0.12	4.37	0.50	5.41	564	Yes
15% RW	7.37	0.30	7.3×10^{-5}	1.3×10^{-3}	2.0×10^{-4}	8.6×10^{-2}	9.8×10^{-2}	5.23	0.17	6.70	1.5×10^{-2}	0.12	6.03	1.1×10^{-2}	6.05	32.7	Yes
20% RW	6.74	0.37	1.7×10^{-5}	7.0×10^{-3}	2.9×10^{-4}	0.11	0.13	4.92	0.16	8.00	1.5×10^{-2}	0.12	5.92	2.5×10^{-3}	5.93	24.1	Yes
30% RW	6.30	0.53	–	2.0×10^{-2}	5.6×10^{-4}	0.17	0.18	4.31	0.15	10.7	1.5×10^{-2}	0.12	5.50	8.4×10^{-4}	5.50	14.9	Yes
50% RW	5.88	0.84	–	5.9×10^{-2}	1.1×10^{-3}	0.27	0.30	3.08	0.11	16.0	1.4×10^{-2}	0.12	4.62	2.6×10^{-4}	4.62	7.33	Yes
80% RW	5.49	1.31	–	0.18	2.5×10^{-3}	0.43	0.47	1.23	6.1×10^{-2}	24.0	1.4×10^{-2}	0.12	3.40	7.8×10^{-5}	3.40	3.14	Yes
River Water**	5.28	1.62	–	0.34	3.6×10^{-3}	0.54	0.59	–	2.7×10^{-2}	29.5	1.4×10^{-2}	0.12	2.74	3.6×10^{-5}	2.74	1.87	No†

* All analytes are reported as the total concentration of all species in mmol/kg, except for HCO_3^- and CO_3^{2-}, which are the concentrations of only those species. DIC indicates dissolved inorganic carbon. Total Alkalinity (TA) is given in mEq/kg. Concentrations below 10^{-6} mmol are not reported.

** Groundwater and river water compositions are derived from the model described in the text and denoted by the blue and red arrows, respectively, along the pH axes in Fig. 3A and 3B.

‡ Mixtures of river water and groundwater with the proportion of river water (RW) in the mixture indicated.

† Yes/No indicates whether evaporation of the mixed water using the model code provided by Toner and Catling (2019), modified only by increasing pCO_2 from 0.1 to 1 bar, results in a concentrated solution with $Fe(CN)_6^{4-} \geq Fe^{2+}$.

with lacustrine and/or restricted shallow marine basins. Given the focus of this contribution, a discussion of the latter is most appropriate. Recently, Sasselov et al. (2020) reviewed the case for why lakes might well be thought of as incubators for the origin of life on planetary surfaces. In lake settings, the combination of access to (1) the critical chemical components of atmospheric hydrogen cyanide (HCN), dissolved iron, and reduced sulfur; (2) near-surface energy sources in the form of ultraviolet light and heat from bolide impacts and igneous activity; and (3) climatically forced wet–dry cycles to concentrate feedstock chemicals would enable prebiotic "cyanosulfidic chemistry" to proceed toward the synthesis of nucleotides, amino acids, and lipid precursors (Patel et al. 2015). Sasselov et al. (2020) discuss evidence for the existence of Martian lacustrine paleoenvironments that could have hosted habitats suitable to cyanosulfidic chemistry, concluding that such conditions were not only possible, but likely.

Within this context, it is worth considering the question of which specific aspects of Martian lake chemistry might have favored (or disfavored) the success of known prebiotic synthesis pathways on the ancient surface of Mars. Toner and Catling (2019) focused on the chemistry of carbonate-rich lakes on the early Earth to evaluate the behavior of atmospherically derived hydrogen cyanide in closed-basin, evaporative lakes fed by runoff derived from weathering of the Earth's early crust. They concluded that ferrocyanide salts (i.e., ferrous iron salts of cyanide) could have been formed by evaporation, providing a concentrated feedstock molecule for subsequent origin of life chemistry. The specific conditions favoring the concentration of these salt compounds from initially dilute lake water include a high partial pressure of HCN gas in the atmosphere over the lake, Fe^{2+} concentrations of ~0.1 mmol, quasi-neutral pH, and low temperature (≤25 °C), which favor the dissociation of HCN(*aq*) to H^+ and CN^-, high carbonate alkalinity to counteract acidity derived from a high pCO_2 atmosphere, and a TA/Me^{2+} ratio that enables pH to increase during evaporation, resulting in the formation of dissolved $Fe(CN)_6^{4-}$ and the precipitation of Na-ferrocyanide salt in the end stages of evaporation.

Based on these criteria, lakes with high carbonate alkalinity on the ancient surface of Mars also seem well suited to the generation of chemical conditions that would favor prebiotic synthesis. Drawing on the chemical scenario described in the previous section, one can imagine that cold, relatively low-pH rivers and streams, acidified by atmospheric CO_2 (± sulfur sourced from volcanic emissions), would have carried dissolved HCN(*aq*), DIC, and dissolved Fe^{2+} from catchment systems to lake basins. There, in shallow shoreline settings above and below the sediment–water interface, interaction with high-pH, high-alkalinity groundwater could have the effect of creating a mixed fluid with the properties needed to form Na-ferrocyanide upon evaporation. Table 1 shows mixed fluid chemistries that achieve $Fe(CN)_6^{4-} \geq Fe^{2+}$ during evaporation, evaluated using the model published in Toner and Catling (2019). This is a necessary precondition to the formation of Na-ferrocyanide salt, and as indicated, mixtures of Martian river and groundwater readily achieve this state.

Notably, lakes with high carbonate alkalinity also have the unique ability to concentrate dissolved phosphate, which is required for adding phosphate groups to organic molecules (phosphorylation) to make nucleotides or adenosine phosphates (Sasselov et al. 2020). In carbonate-rich lakes with high TA/Me^{2+}, the removal of dissolved Ca^{2+} from solution by calcite precipitation allows dissolved PO_4^{3-} to build up to remarkably high (hundreds of millimole) concentrations during evaporation because, under such conditions, PO_4^{3-} is not limited by apatite solubility (Ingalls et al. 2020; Toner and Catling 2020).

Further laboratory and modeling research are needed to form a more complete understanding of how favorable this kind of origin of life chemistry is under the surface conditions on early Mars. For example, the unknown role of exotic oxidants (e.g., oxyhalogens, radical species) in early

Martian geochemical cycles, and the possibility that Mars experienced only brief climate optima within an otherwise dominantly cryogenic state, are two examples of factors or conditions that might have acted to limit or constrain possibilities for the origin and evolution of life on Mars. Fortunately, a great many of these questions are likely to be resolved in the next decade with the return of samples from Jezero Crater by the international Mars Sample Return campaign. These samples are being collected from a paleoenvironmental setting that is being characterized by the *Perseverance* rover in greater detail than ever before possible (e.g., Liu et al. 2022). The recognition of a preserved record of prebiotic chemical processes in such samples could provide as much insight into life's origins as a biological record would provide regarding its earliest forms and abundance—both are worthy goals in the search for a deeper understanding of life in the Universe.

ACKNOWLEDGMENTS

JA Hurowitz, DC Catling, and WW Fischer gratefully acknowledge funding from the Simons Collaboration on the Origin of Life (SCOL), award numbers 572786, 511570, and 554187, respectively. DC Catling also acknowledges funding from NASA grant 80NSSC21K0149. We gratefully acknowledge insightful reviews by Eva Stüeken and an anonymous reviewer.

REFERENCES

Baldridge AM and 9 coauthors (2009) Contemporaneous deposition of phyllosilicates and sulfates: using Australian acidic saline lake deposits to describe geochemical variability on Mars. Geophysical Research Letters 36: L19201, doi: 10.1029/2009GL040069

Catling DC, Kasting JF (2017) Atmospheric Evolution on Inhabited and Lifeless Worlds. Cambridge University Press, 595 pp, doi: 10.1017/9781139020558

Ehlmann BL, Edwards CS (2014) Mineralogy of the Martian surface. Annual Review of Earth and Planetary Sciences 42: 291-315, doi: 10.1146/annurev-earth-060313-055024

Farley KA and 232 coauthors (2014) In situ radiometric and exposure age dating of the Martian surface. Science 343, doi: 10.1126/science.1247166

Fassett CI, Head JW (2008) Valley network-fed, open-basin lakes on Mars: distribution and implications for Noachian surface and subsurface hydrology. Icarus 198: 37-56, doi: 10.1016/j.icarus.2008.06.016

Goudge TA, Fassett CI, Head JW, Mustard JF, Aureli KL (2016) Insights into surface runoff on early Mars from paleolake basin morphology and stratigraphy. Geology 44: 419-422, doi: 10.1130/G37734.1

Grotzinger JP and 19 coauthors (2005) Stratigraphy and sedimentology of a dry to wet eolian depositional system, Burns formation, Meridiani Planum, Mars. Earth and Planetary Science Letters 240: 11-72, doi: 10.1016/j.epsl.2005.09.039

Grotzinger JP and 46 coauthors (2015) Deposition, exhumation, and paleoclimate of an ancient lake deposit, Gale crater, Mars. Science 350, doi: 10.1126/science.aac7575

Gysi AP, Stefánsson A (2011) CO_2–water–basalt interaction. Numerical simulation of low temperature CO_2 sequestration into basalts. Geochimica et Cosmochimica Acta 75: 4728-4751, doi: 10.1016/j.gca.2011.05.037

Gysi AP, Stefánsson A (2012) CO_2–water–basalt interaction. Low temperature experiments and implications for CO_2 sequestration into basalts. Geochimica et Cosmochimica Acta 81: 129-152, doi: 10.1016/j.gca.2011.12.012

Horgan BHN, Anderson RB, Dromart G, Amador ES, Rice MS (2020) The mineral diversity of Jezero crater: evidence for possible lacustrine carbonates on Mars. Icarus 339: 113526, doi: 10.1016/j.icarus.2019.113526

Hu R, Thomas TB (2022) A nitrogen-rich atmosphere on ancient Mars consistent with isotopic evolution models. Nature Geoscience 15: 106-111, doi: 10.1038/s41561-021-00886-y

Ingalls M and 5 coauthors (2020) P/Ca in carbonates as a proxy for alkalinity and phosphate levels. Geophysical Research Letters 47: e2020GL08804, doi: 10.1029/2020GL088804

Kite ES, Daswani MM (2019) Geochemistry constrains global hydrology on early Mars. Earth and Planetary Science Letters 524: 115718, doi: 10.1016/j.epsl.2019.115718

Kite ES, Steele LJ, Mischna MA, Richardson MI (2021) Warm early Mars surface enabled by high-altitude water ice clouds. Proceedings of the National Academy of Sciences 118: e2101959118, doi: 10.1073/pnas.2101959118

Kusakabe M and 5 coauthors (2019) Enrichment of ferrous iron in the bottom water of Lake Nyos. Journal of African Earth Sciences 150: 37-46, doi: 10.1016/j.jafrearsci.2018.10.014

Liu Y and 70 coauthors (2022) An olivine cumulate outcrop on the floor of Jezero crater, Mars. Science 377: 1513-1519, doi: 10.1126/science.abo2756

Mangold N and 38 coauthors (2021) Perseverance rover reveals an ancient delta-lake system and flood deposits at Jezero crater, Mars. Science 374: 711-717, doi: 10.1126/science.abl4051

McLennan SM, Grotzinger JP, Hurowitz JA, Tosca NJ (2019) The sedimentary cycle on early Mars. Annual Review of Earth and Planetary Sciences 47: 91-118, doi: 10.1146/annurev-earth-053018-060332

Michalski JR and 5 coauthors (2022) Geological diversity and microbiological potential of lakes on Mars. Nature Astronomy 6: 1133-1141, doi: 10.1038/s41550-022-01743-7

Patel BH, Percivalle C, Ritson DJ, Duffy CD, Sutherland JD (2015) Common origins of RNA, protein and lipid precursors in a cyanosulfidic protometabolism. Nature Chemistry 7: 301-307, doi: 10.1038/nchem.2202

Pogge von Strandmann PAE and 5 coauthors (2017) Lithium isotopes in speleothems: temperature-controlled variation in silicate weathering during glacial cycles. Earth and Planetary Science Letters 469: 64-74, doi: 10.1016/j.epsl.2017.04.014

Rampe EB and 41 coauthors (2020) Mineralogy and geochemistry of sedimentary rocks and eolian sediments in Gale crater, Mars: a review after six Earth years of exploration with *Curiosity*. Geochemistry 80: 125605, doi: 10.1016/j.chemer.2020.125605

Sasselov DD, Grotzinger JP, Sutherland JD (2020) The origin of life as a planetary phenomenon. Science Advances 6, doi: 10.1126/sciadv.aax3419

Thorpe MT, Hurowitz JA, Siebach KL (2021) Source-to-sink terrestrial analogs for the paleoenvironment of Gale crater, Mars. Journal of Geophysical Research: Planets 126: e2020JE006530, doi: 10.1029/2020JE006530

Toner JD, Catling DC (2019) Alkaline lake settings for concentrated prebiotic cyanide and the origin of life. Geochimica et Cosmochimica Acta 260: 124-132, doi: 10.1016/j.gca.2019.06.031

Toner JD, Catling DC (2020) A carbonate-rich lake solution to the phosphate problem of the origin of life. Proceedings of the National Academy of Sciences 117: 883-888, doi: 10.1073/pnas.1916109117

Tosca NJ, Ahmed IAM, Tutolo BM, Ashpitel A, Hurowitz JA (2018) Magnetite authigenesis and the warming of early Mars. Nature Geoscience 11: 635-639, doi: 10.1038/s41561-018-0203-8

Tosca NJ, Tutolo BM (2023) How to make an alkaline lake: fifty years of chemical divides. Elements 19: 15-21

Wordsworth R and 6 coauthors (2021) A coupled model of episodic warming, oxidation and geochemical transitions on early Mars. Nature Geoscience 14: 127-132, doi: 10.1038/s41561-021-00701-8 ■